Energy Conversion and Management 87 (2014) 19–28

Contents lists available at ScienceDirect

Energy Conversion and Management

journal homepage: www.elsevier.com/locate/enconman

Cross-flow membrane-based enthalpy exchanger balanced and unbalanced flow

R. Sebai *, R. Chouikh, A. Guizani

Center for Energy Research and Technology (CRTEn), BP 95, Hamamlif 2050, Tunisia

ARTICLE INFO

Article history:
Received 13 March 2014
Accepted 1 July 2014
Available online 18 July 2014

Keywords:
Heat and mass transfer
Membrane
Balanced and unbalanced flow

ABSTRACT

In order to deepen the understanding of the main phenomena governing the membrane based energy recovery ventilators performance, we present a three dimensional numerical study of the mechanisms of heat and mass transfer in a cross-flow heat exchanger with balanced and unbalanced flow. This work involves the use of a control-volume method and solves the set of Navier–Stokes equations in the air streams and as well as in the membrane core. The results are compared to literature available data and the agreement is seen to be satisfactory. The effect of operating parameters such as the Reynolds number, volume flow rates and temperature on the performance of the heat exchanger are also investigated.

1. Introduction

With the continuous increase in the prices of energy, the need for optimizing the energy recovery systems is in strong growth. It is one of the main attractive solutions to face the fossil energies rising prices and to reduce the impact of the human activity on the environment. Thermal recovery is done, either on "free" energies (solar energy), or on thermal coming "waste" from industrial processes or thermal systems. The heat recovery systems allow recovering the heat produced by equipment for then redistributing it via installations of ventilation. The extracted heat from the buildings by ventilation is thus transferred to the new air entering the building. For hygienic consideration, conditioning ventilation air constitutes 20–40% of thermal load for ordinary buildings and can be even higher in special buildings (hospital, factories, kitchen...) which require 100% outdoor air to meet ventilation standards [1].

Reducing this part of energy is crucial for the reduction of energy consumption of the whole HVAC system. There are many studies in literature aimed at improving the HVAC systems in buildings while reducing the energy consumption with the positive environmental impacts. However, the numerical investigations of unbalanced flow, which is more realistic, have been, up to now insufficiently studied.

One of the early works is the numerical study of the enthalpies wheel made by Sankar Nair et al. in 1998. They considered an axial heat dispersion and longitudinal matrix conduction and they solved the wheel heat/mass exchanger problems using a finite difference approach [2]. The predicted recovery effectiveness has a value of about 75%. Rotating factors of the enthalpy were considered in the calculating method by Frauhammer et al. [3]. They studied the efficiency of condensation and evaporation in a regenerative air-to-air heat exchanger.

In 1997, solid adsorbents such as activated carbon–methanol, zeolite–water, $CaCl_2$–NH_3 and hydride-hydrogen was integrated with shell, tube, flat pipe, flat plate, and plate-fin heat exchanger to carry out the heat and mass recovery synchronously (Wang et al. [4]; Hachemi [5]). The main disadvantages of these earlier plate enthalpy exchangers are the huge thermal resistance between adsorbents and fins, lower adsorption and intermittence of regenerating of the saturated adsorbents. Wang et al. [6] developed one type of spiral plate type absorber exchanger made of two parallel stainless steel welded plates and adsorbents with the advantages of higher adsorption, compact size, higher thermal transfer, easier manufacturing, and cheaper price.

Manz and Huber [6] have presented a mechanical building ventilation unit that combines two functions: fluid transport and heat recovery. They measured in an experimental set-up the air flow rates, temperatures; air humidity's and pressure differences. The influence of the heat exchanger geometry variation on thermal efficiency was predicted by these authors. They proved that the thermal insulation is most effective where the temperature differences between the aluminum profile and ambient space are at a maximum.

In order to intensify the convective mass transfer coefficients on membrane surfaces, Zhang [7] has used a cross-corrugated

* Corresponding author. Tel.: +216 22583832; fax: +216 70860434.
E-mail address: ramzi4400@yahoo.fr (R. Sebai).

http://dx.doi.org/10.1016/j.enconman.2014.07.002
0196-8904/

Nomenclature

A_t	cross section
C_p	specific heat (kJ kg^{-1} K^{-1})
D	diffusivity (m^2/s)
D_h	hydraulic diameter
h	convective heat transfer coefficient (kW m^{-2} K^{-1})
k	convective mass transfer coefficient (m/s)
ℓ	width canal (m)
L	length canal (m)
$\dot{m}$	mass flow rate of air streams (kg s^{-1})
$\dot{m}_w$	mass flow rate of moisture flow (kg m^{-2} s^{-1})
Reu and Rev	reynolds number respectively in the supply and exhaust canal
P	pressure
Pr	Prandtl number $\mathrm{Pr} = \frac{v}{\alpha}$
Sc	Schmidt number $Sc = \frac{v}{D_{va}}$
T	temperature (K)
u, v	velocity (m/s) for supply and exhaust side respectively
U, V	dimensionless velocity
w	water uptake (kg/kg)
x, y, z	coordinates (m)
X, Y, Z	dimensionless coordinates

Greek symbols

α	thermal diffusivity
δ_m	membrane thickness (m)
δ_e	height of Exhaust canal (m)
δ_s	height of Supply canal (m)
μ	dynamic viscosity (Pa s)
ρ	density of dry air (kg/m^3)
ϕ	air relative humidity
θ	dimensionless temperature
ω	humidity ratio (kg moisture/kg air)
λ	thermal conductivity (kW m^{-1} K^{-1})

Subscripts

a	air
e	exhaust air side
h	heat
i	inlet
m	mass, membrane
o	outlet
v	vapor
s	supply air side

triangular ducts that provide high mass transfer capabilities in membrane related gas separations. He examined the vapor mass fractions, the velocity, and the turbulent kinetic energy in the three-dimensional complex domain. The friction factors and the mean Sherwood numbers are calculated and correlated with Reynolds numbers, for uniform mass fraction boundary conditions.

Zhang [8] has investigated numerically and experimentally the heat and mass transfer mechanisms in a cross-flow parallel plate membrane-based enthalpy exchanger for heat and moisture recovery from exhaust air streams. The author numerically obtained the real boundary conditions on the exchanger surfaces of the coupled equations that govern the transfer of momentum, thermal energy and moisture in the two cross-flow air streams and through the membrane. On another hand, in the experimental contribution, he found that the fully developed Sherwood numbers are nearly equal to the fully developed Nusselt numbers.

Kadylak et al. [9] have presented an experimental work in which the latent effectiveness and the latent Number of Transfer Units (NTUs) for mass transfer in membrane humidity exchangers were applied to Proton Exchange Membrane Fuel Cell (PEMFC) membrane humidifiers. Their principal result shows that the use of a constant vaporization enthalpy taken from a low reference temperature in the Clausius–Clapeyron equation causes the deviation of the predicted outlet conditions from the true conditions.

Zhang [10] has presented a numerical study on laminar forced flow and heat mass transfer in sinusoidal plate-fin small passages encountered in compact heat mass exchangers. The heat conduction and mass diffusion in the fins and heat and moisture convection in the fluid were analyzed simultaneously. Their fully developed Nusselt and Sherwood numbers under various aspect ratios and fin conductance parameters are calculated.

Fernández-Seara et al. [11] have shown and discussed the experimental analysis of an air-to-air heat recovery with a sensible polymer plate heat exchanger (PHE) for balanced ventilation systems in residential buildings. An experimental facility was designed to reproduce the typical outdoor and exhaust air conditions with regard to temperature and humidity. The outlet exhaust air temperature was lower than its dew-point temperature and water condensation took place throughout the tests. The experimental results indicate that the heat transfer rate in the PHE decreases almost linearly as the inlet fresh air temperature increases.

Zhang et al. [12] presented a numerical and experimental work dealing with the effect of the water vapor sorption properties of the plate materials on the performance of the membrane. Their results indicate that the moisture resistance through plates is co-determined by thickness, sorption slope, and sorption potential. Besides, they noted that the moisture diffusivity in various materials is of the same order. Hence, in case the plate thickness is fixed, the higher the sorption slopes are, the higher the latent performance is obtained.

With finger-like macro voids asymmetric porous membranes structure, Zhang [13] has presented a study on heat and mass transfer. This study gave a more detailed investigation of the thermal and mass diffusion through these membranes, with the help of scanning electron microscope (SEM) observations of membrane surface and cross-sectional structures. Results show that the effective diffusivity of the membrane has been extensively improved due to the existence of more than 70,000 per meter large finger-like voids inside.

Mahmud et al. [14] have presented a membrane energy exchanger (RAMEE) system. It consists of two counter-cross flow liquid-to-air membrane energy exchangers. The RAMEE system exchanges the sensible and latent energy between the supply and exhaust air streams. A micro-porous membrane separates the air and desiccant solution streams and allows heat and water vapor exchange between the two streams. They also proved that the system performs better in the winter season than in the summer season implying more energy savings during the winter operations.

Zhang et al. [15] carried out an investigation dealing with the conjugate heat and mass transfer in asymmetric porous membranes in all entry regions. The momentum, energy and mass equations are solved directly without assumptions of hydraulically, thermally or concentration-ally fully developed flow. The effects of three typical flow arrangements: co-current, counter and cross

flow, on the boundary conditions and the consequent Nusselt and Sherwood numbers in the channels are evaluated.

To understand the reasons for performance limitations in order to optimize system performance, Zhang et al. [16] studied the properties of sensible heat transfer processes and coupled heat and mass transfer processes. The condition of flow matching is achieved when the heat capacities of the two fluids in the heat transfer process and the coupled heat and mass transfer process are identical. Analytical solutions of heat transfer resistance and mass transfer resistance were then derived. Furthermore, losses were seen to occur during the heat and mass transfer processes due to limited transfer capability, flow mismatching, and parameter mismatching.

Vaz et al. [17] presented an experimental and numerical study of earth–air heat exchangers, through the use of thermal energy contained in the soil. They investigated the variation of air temperature inside the ducts, for an annual cycle. The results of temperature fields predicted numerically were compared with the experimental results. They proved that the soil is a reservoir of energy derived from solar radiation, usable to reduce the consumption of energy in the process of renewal of air in built environments.

Al-Waked et al. [18] developed a CFD model which supports conjugate heat and mass transfer problem representation across the membrane of air-to-air energy recovery heat exchangers. The simulation results have shown that counter-flow configuration has greater sensitivity to the mesh centre perpendicular distance from the membrane when compared to the other two flow configurations (cross-/parallel-flow). To obtain accurate results, they have found that the perpendicular distance value should be in a close proximity to the membrane thickness. The sensible effectiveness, latent effectiveness and pressure drop across the membrane heat exchanger are presented and analyzed.

In the current investigation is presented a numerical study of comparison between the effect of balanced and unbalanced flows on the mechanisms of heat and mass transfer in a cross-flow heat exchanger, whose heat-transferring surface is an exchanging fine membrane based enthalpy exchangers. This membrane process allows the recovery of heat in its two forms sensible and latent. Through volume control simulation, the heat and mass transfer mechanism and performance of the system are studied. The performance of the exchanger is studied in terms of sensible, latent and total effectiveness. The temperature, humidity fields for both the supply and exhaust flows are obtained for different Reynolds numbers.

2. Theoretical model

The membrane-based enthalpy exchanger is a main component of energy recovery technology known as heat Recovery Ventilators or Energy Recovery Ventilators. The two air streams flowing across a water-permeable membrane are arranged such that one air stream is hot and humid while the other air stream is relatively dry and cool. Due to the gradients in the temperature and vapor pressure concentration, heat and moisture are transferred across the membrane. The heat and moisture are transported from the hot and humid stream to the membrane surface by convection, followed by conduction of heat and diffusion of moisture through the porous membrane and by convection from the membrane surface to the cold and less humid stream, causing a decrease in temperature and humidity of the supply air stream and hence, both sensible and latent energy are recovered.

A schematic of a unit cell membrane based energy recovery is shown in Fig. 1. The two air streams, the feed and exhaust flow in thin parallel, alternating membrane layers in a cross-flow arrangement, allow heat and moisture transfer from one air stream to the other. The fresh air and the exhaust air flow through the passages in a cross-flow arrangement. The geometries of ducts are summarized as follows: height δ_e for Exhaust canal and δ_s for Supply canal, length L, width ℓ and membrane thickness δ_m.

Contrarily to the co-current flow and counter current flow, the cross-flow configuration does not present a symmetrical plan. Therefore, a three dimensional study is required to analyze the heat and mass transfer. It is to be noted that the average value of the considered general variable Φ is always lower than the two dimensional prediction in which, the heat and mass transport is absent in the third direction. The equations of the studied physical problem, presented in this section, use the nomenclature and coordinate system shown in the Fig. 1.

The major assumptions in the mathematical model are summarized as follows:

- The fluid is Newtonian with constant thermal properties.
- Adsorption of water vapor and membrane material is at equilibrium adsorption-state.
- The heat of sorption is assumed constant and equal to the heat of vaporization.
- Both heat conductivity and water diffusivity in the membrane are constant in range of the operating temperature used in air-conditioning system.
- Heat conduction and vapor diffusion of the two air streams along flow directions (axial) are negligible compared to energy transport and vapor convection by bulk flow.

The flow field is governed by the steady state Navier–Stokes equations, which expresses momentum conservation for a Newtonian fluid. In this study, they are written in Cartesian coordinates and in dimensionless form as follows

$$U\frac{\partial U}{\partial X}+V\frac{\partial U}{\partial Y}+W\frac{\partial U}{\partial Z}=-\frac{\partial \mathrm{P}}{\partial \mathrm{X}}+\mathrm{Pr}\left(\frac{\partial^2 U}{\partial X^2}+\frac{\partial^2 U}{\partial Y^2}+\frac{\partial^2 U}{\partial Z^2}\right) \quad (1)$$

$$U\frac{\partial V}{\partial X}+V\frac{\partial V}{\partial Y}+W\frac{\partial V}{\partial Z}=-\frac{\partial \mathrm{P}}{\partial \mathrm{Y}}+\mathrm{Pr}\left(\frac{\partial^2 V}{\partial X^2}+\frac{\partial^2 V}{\partial Y^2}+\frac{\partial^2 V}{\partial Z^2}\right) \quad (2)$$

$$U\frac{\partial W}{\partial X}+V\frac{\partial W}{\partial Y}+W\frac{\partial W}{\partial Z}=-\frac{\partial \mathrm{P}}{\partial \mathrm{Z}}+\mathrm{Pr}\left(\frac{\partial^2 W}{\partial X^2}+\frac{\partial^2 W}{\partial Y^2}+\frac{\partial^2 W}{\partial Z^2}\right) \quad (3)$$

The dimensionless coordinates are as follows:

$$X=\frac{x}{D_h};Y=\frac{y}{D_h};Z_s=\frac{z}{D_h};Z_e=\frac{z}{D_h};Z_m=\frac{z}{\delta_m};U=\frac{D_h u}{\alpha};$$
$$V=\frac{D_h v}{\alpha};W=\frac{D_h w}{\alpha} \quad (4)$$

We consider the following dimensionless temperatures and humidity:

$$P=\frac{pD_{\mathrm{h}}}{\rho\alpha^2};\theta=\frac{T-T_{ei}}{T_{si}-T_{ei}};\quad \theta_m=\frac{T_m-T_{ei}}{T_{si}-T_{ei}};\quad \omega=\frac{w-w_{ei}}{w_{si}-w_{ei}};$$
$$\omega_m=\frac{w_m-w_{ei}}{w_{si}-w_{ei}} \quad (5)$$

where T_{si} is the inlet temperature of the supply air (hot and humid), and T_{ei} is the inlet temperature of the exhaust air (cool and dry). w_{si} is the inlet humidity of the supply air and w_{ei} is the inlet humidity of the exhaust air.

D_h is the hydraulic diameter of the considered channel $\left(D_h=\frac{4A_{\mathrm{t}}}{P_{\mathrm{e}}}\right)$.

where A_t is the cross section and P_e is the perimeter of considered channel.

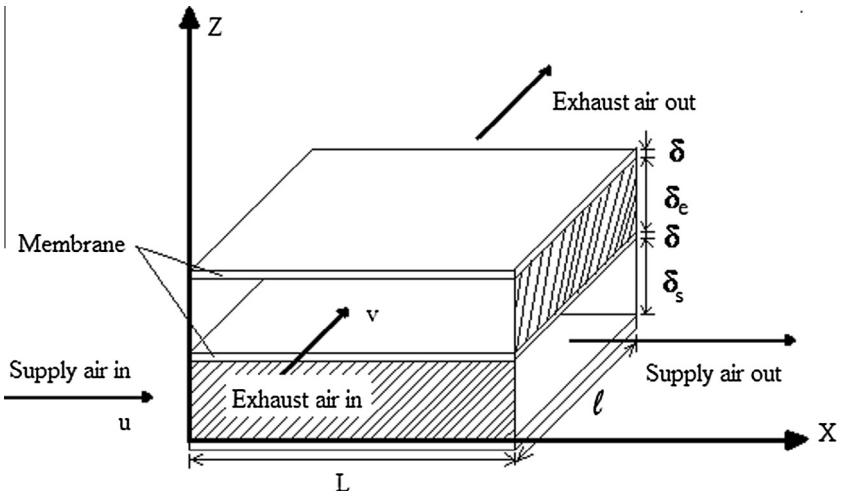

Fig. 1. Schematic of a cross-flow enthalpy exchanger with membrane cores.

An enthalpy and mass balance has been established for a control volume to obtain the differential equation (convecto-diffusive equation) which describes the heat and mass transfer in the exchanger.

The fresh air, which is usually hot and humid, flows along *x*-axis while the exhaust air, which is usually cool and dry, flows along the *y*-axis. Even though the coordinate system, inlet and boundaries conditions are different, the equation governing the transport phenomena are in the same form for the two passages.

For cross flow membrane energy recovery, the dimensionless equations can be written as follows:

2.1. Supply side

$$\text{Energy conservation} \ : \ U\frac{\partial\theta}{\partial X}+V\frac{\partial\theta}{\partial Y}+W\frac{\partial\theta}{\partial Z}=\frac{\partial^2\theta}{\partial Y^2}+\frac{\partial^2\theta}{\partial Z^2} \tag{6}$$

$$\text{Water vapor conservation} \ : \ U\frac{\partial\omega}{\partial X}+V\frac{\partial\omega}{\partial Y}W\frac{\partial\omega}{\partial Z} = \frac{\mathrm{Pr}}{Sc}\frac{\partial^2\omega}{\partial Y^2}+\frac{\mathrm{Pr}}{Sc}\frac{\partial^2\omega}{\partial Z^2} \tag{7}$$

Boundary conditions:

Inlet conditions for supply air

$$X=0 \ \rightarrow \ \theta_i(Y,Z_s)=1 \quad and \quad \omega_i(Y,Z_s)=1 \tag{8}$$

Outlet conditions for supply air

$$X=1 \ \rightarrow \ \frac{\partial\theta}{\partial X}=\frac{\partial\omega}{\partial X}=0 \tag{9}$$

Adiabatic boundary conditions on walls

$$Y=0 \quad or \quad Y=1, \quad \frac{\partial\theta}{\partial Y}=\frac{\partial\omega}{\partial Y}=0 \tag{10}$$

2.2. Exhaust side

Energy conservation:

$$U\frac{\partial\theta}{\partial X}+V\frac{\partial\theta}{\partial Y}+W\frac{\partial\theta}{\partial Z}=\frac{\partial^2\theta}{\partial X^2}+\frac{\partial^2\theta}{\partial Z^2} \tag{11}$$

Water vapor conservation:

$$U\frac{\partial\omega}{\partial X}+V\frac{\partial\omega}{\partial Y}+W\frac{\partial\omega}{\partial Z}=\frac{\mathrm{Pr}}{Sc}\frac{\partial^2\omega}{\partial X^2}+\frac{\mathrm{Pr}}{Sc}\frac{\partial^2\omega}{\partial Z^2} \tag{12}$$

Boundary conditions:

Inlet conditions for exhaust air

$$Y=0 \ \rightarrow \ \theta_i(X,Z_e)=0 \quad and \quad \omega_i(X,Z_e)=0 \tag{13}$$

Outlet conditions for exhaust air

$$Y=1 \ \rightarrow \ \frac{\partial\theta}{\partial Y}=\frac{\partial\omega}{\partial Y}=0 \tag{14}$$

Adiabatic boundary conditions on walls

$$X=0 \quad or \quad X=1, \quad \frac{\partial\theta}{\partial X}=\frac{\partial\omega}{\partial X}=0 \tag{15}$$

2.3. Membrane

The steady state heat transfer in membrane is written as:

$$\frac{\partial^2\theta_m}{\partial X^2}+\frac{\partial^2\theta_m}{\partial Y^2}+\frac{\partial^2\theta_m}{\partial Z_m^2}=0 \tag{16}$$

The steady state moisture transfer in membrane is written as:

$$\frac{\partial^2\omega_m}{\partial X^2}+\frac{\partial^2\omega_m}{\partial Y^2}+\frac{\partial^2\omega_m}{\partial Z_m^2}=0 \tag{17}$$

Heat and moisture transfer in the *x* and *y* directions are considered negligible due to the small membrane thickness (10^{-4} m) and also to the transversal thermal and mass gradients between the two air steams. Then, heat and mass transfer in membrane can be simplified to one-dimensional equation.

$$\frac{\partial^2\theta_m}{\partial Z_m^2}=0 \qquad \frac{\partial^2\omega_m}{\partial Z_m^2}=0 \tag{18}$$

where θ and θ_m are respectively the dimensionless temperatures of air and membrane. ω_m is the dimensionless water uptake of the membrane, ω is the dimensionless humidity ratio of the air.

Boundary conditions are given by:

On membrane surface for supply side

$$Z_s=0 \ or \ Z_s=1, \ \theta_m(X,Y)=\theta_{ms} \ and \ \omega_m(X,Y)=\omega_{ms} \tag{19}$$

On membrane surface for exhaust side

$$Z_e=0 \ or \ Z_e=1, \ \theta_m(X,Y)=\theta_{me} \ and \ \omega_m(X,Y)=\omega_{me} \tag{20}$$

Adiabatic boundary conditions for membrane side

$$X=0 \quad or \quad X=1 \rightarrow \frac{\partial\theta_m}{\partial X}=\frac{\partial\omega_m}{\partial X}=0 \tag{21}$$

$$Y=0 \quad or \quad Y=1 \rightarrow \frac{\partial\theta_m}{\partial Y}=\frac{\partial\omega_m}{\partial Y}=0 \tag{22}$$

3. Numerical results

The developed CFD code is structured around numerical algorithm that solves equations representing physical conservation laws in order to obtain the heat and mass fields in the two ducts and the membrane. The mathematical model of heat and mass transfer in membrane based energy recovery are solved numerically using the control volume scheme and solved by using the Successive Over Relaxation method (SOR) with Chebyshev acceleration [19].

This method is based on the conservative form of the governing differential equation which describes the convection–diffusion situation. Since the convective–diffusive equation must satisfy the continuity equation:

$$\frac{\partial}{\partial x_j}(\rho u_i) = 0 \tag{23}$$

The general differential equation given by

$$\rho u_i \frac{\partial \Phi}{\partial x_i} = \frac{\partial}{\partial x_j}\left(\Gamma \frac{\partial \Phi}{\partial x_i}\right) \tag{24}$$

can also be written as a convecto-diffusive equation: (by combining the precedent equations)

$$\frac{\partial(\rho u_i \Phi)}{\partial x_i} = \frac{\partial}{\partial x_j}\left(\Gamma \frac{\partial \Phi}{\partial x_i}\right) \quad \Rightarrow \quad \frac{\partial}{\partial x_j}\left(\rho u_i \Phi - \Gamma \frac{\partial \Phi}{\partial x_i}\right) = 0 \tag{25}$$

The first term is the convection term and the second is the diffusion term. Under these circumstances, the basic rule about the sum of the coefficients of the corresponding algebraic equation (discredited equation) continues to apply [20].

As the momentum equation is formulated in terms of the primitive variables (velocity and pressure) the iterative procedure includes a pressure correction calculation method to solve the pressure–velocity coupling. The code uses the SIMPLE technique (Patankar [21]) for the pressure and velocity corrections.

The convergence is reached when each variable satisfy the following criterion:

$$\sum_{i,j} |\phi_{i,j}^{n+1} - \phi_{i,j}^{n}| \Big/ \sum_{i,j} |\phi_{i,j}^{n}| \leqslant 10^{-4} \tag{26}$$

where ϕ stands for the simulated variable and n is the iteration order.

The adopted method has been previously successfully utilized and verified for solving more complex problems like the combined heat and mass transfer in an inclined cavity [22] and modeling of concentration and current in a fuel cell [23,24].

The numerical results are validated qualitatively with those of Zhang [8] for the same configuration of flow. Figs. 2 and 3 (respectively 4 and 5) show a comparison between our results and those of Zhang [8] in terms of velocity contour (respectively in terms of temperature contour) in the mid section of the channel. Both figures of dimensionless velocity (Figs. 2 and 3) are almost similar. It is observed that, the contours of velocity are maximal and nearly as rectangles in the duct centre. Besides, in the four corners, the dimensionless velocities are near zero. The dimensionless temperature contour (Figs. 4 and 5) are similar and symmetric to the flow direction. The corresponding velocity vectors field is presented in Fig. 6. The agreement between these results is satisfactory.

We present our results for both balanced and unbalanced flow in the channels and in the membrane. The effectiveness of the system is also investigated in order to optimize the operating parameters.

The considered geometrical and physical parameters of the membrane based energy recovery ventilator are listed in Table 1.

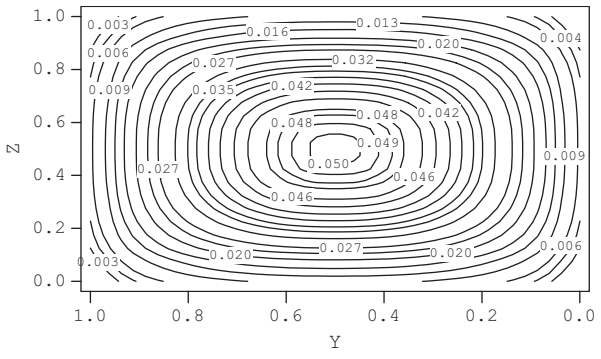

Fig. 2. The (*Y*–*Z*) velocity contours on channel cross-section.

3.1. Balanced flow

In a balanced flow, the flow rate of the supply channel is equal to the flow rate of the exhaust channel. For equal values of velocities u and v; at $z = 5 \cdot 10^{-3}$ m, the temperature profiles for supply air (resp. exhaust air) at $y = 0.25$ m (resp. at $x = 0.25$ cm) are plotted in Fig. 7 (resp. Fig. 8). These figures, present three temperature profiles for Reynolds number Reu = Rev ranging from 10^2 to 10^3. For Reu = Rev = 10^2, the temperature variation in the entry for $0 < x < 0.1$ m is constant and is decreasing elsewhere. It is observed that the temperature and humidity profiles decrease along the x axis in the supply side and increase along the y axis in the exhaust side. For relatively low Reynolds numbers, the variations in temperature are very important for both channels due to the fact that an important residence time and weak velocity leave more time to thermal and mass transfer in both channels. For large Reynolds numbers, higher than 10^3, the temperature profiles become constant, the outlet value of temperature is almost equal to inlet value of temperature for both supply air and exhaust air. The variations in temperature between the entry and the exit in both channels are more important when the Reynolds number is weak.

In the membrane, the temperature profiles along the z axis at $x = y = 0.25$ m are depicted in Fig. 9. The temperature profiles are plotted along the x axis at $y = 0.25$ m and $z = 10^{-4}$ m in Fig. 10. The vertical variation in temperature between the two heat-transferring membrane surfaces is seen to be very important for relatively low Reynolds numbers. For Reu = Rev = 10^2, the vertical variation in temperature is equal to 0.1 °C and for Reu = Rev = 10^3, it is equal to 0.04 °C (Fig. 9). The horizontal variation in temperature is equal to 8.2 °C for Reu = Rev = 10^2, and is equal to 5 °C for Reu = Rev = 10^3 (Fig. 10). However, for Reynolds numbers higher than 10^3, the variation in temperature between the two heat-transferring membrane surfaces becomes very weak. Thus, for small Reynolds number, more time is needed for heat and mass exchange between the two flow channels. It is worth noting that the air-to-air heat exchange efficiency decreases when the Reynolds number is augmented accordingly.

3.2. Unbalanced flow

For unbalanced flow, the flow rate of the supply channel and the flow rate of the exhaust channel are different. The unbalanced flow addresses special applications as in pressurized rooms where the pressure is superior to the atmospheric one to avoid the entry of dust. For the case of unbalanced flow, we have fixed the Reynolds number in the supply flow channel at Reu = 10^2, which is an optimal value for heat and mass transfers in balanced flow [25], and we have varied the Reynolds number in the exhaust flow channel. These results are plotted in Fig. 11. Reciprocally, we have fixed

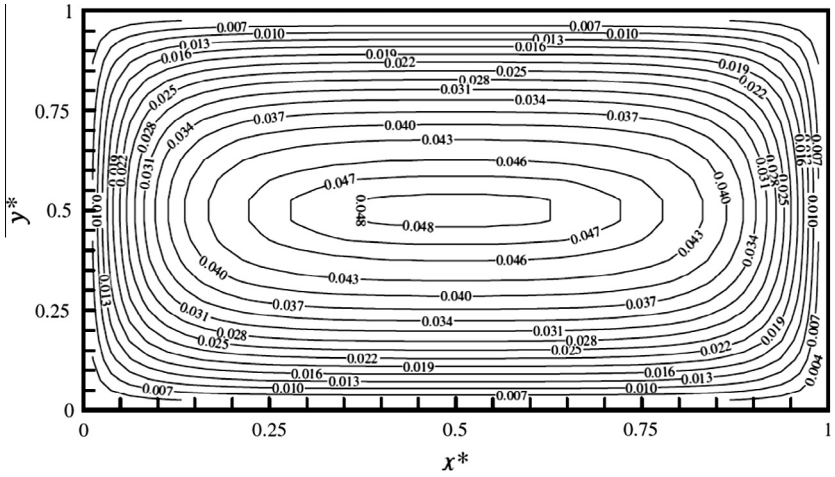

Fig. 3. The (Y–Z) u component velocity contours result of Zhang [8].

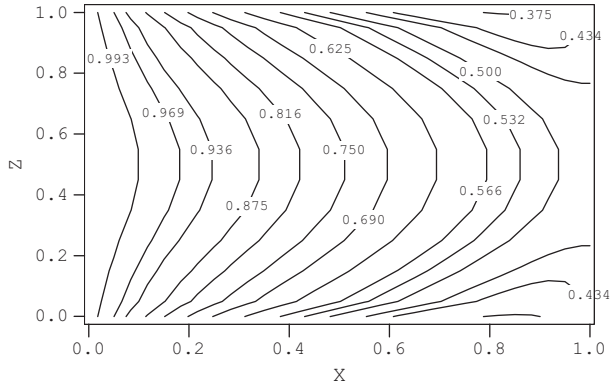

Fig. 4. Dimensionless temperature profile in (X–Y) plane at $Z = \delta_c/2$ for supply air at Reu = Rev = 10^3.

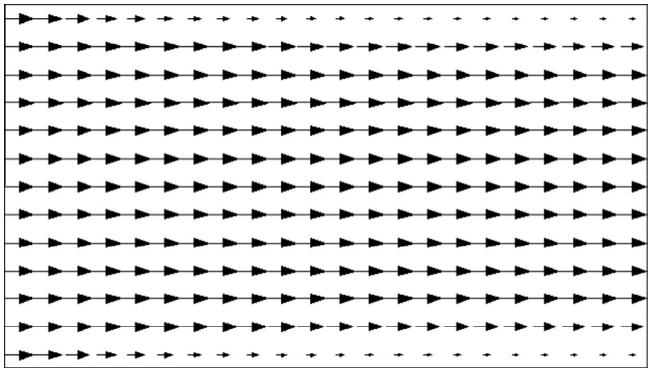

Fig. 6. The (X–Y) velocity vectors field of supply channel at $Z = \delta_c/2$.

the Reynolds number in the exhaust flow channel at Rev = 10^2 and while the Reynolds number in supply flow channel is increased from 10^2 to 10^3 (Fig. 12). The temperatures profiles take an exponential shape, decreasing for the supply channel and increasing for the exhaust channel. For large Reynolds numbers, higher than 10^3, the temperature profiles take a hyperbolic form. It is also observed that when the velocity of flow is gradually increased, the temperature profile reaches quickly its limiting value. In fact, the temperature is lowered more rapidly when the x coordinate is in the range of 0–0.3 m.

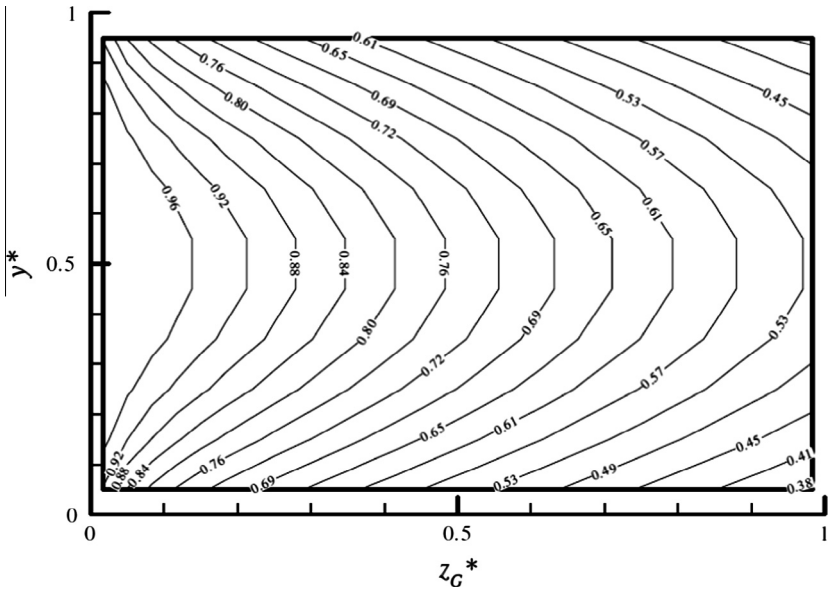

Fig. 5. Dimensionless temperature profile in (X–Y) plane result of Zhang [8].

Table 1
Some parameters of the membrane-based enthalpy exchanger for model validation.

Symbol	Value	Unit
C_{pw}	1.009	(kJ/kg K)
l	50.0E−02	(m)
L	50.0E−02	(m)
W_{max}	0.3	(kg/kg)
δ_m	2.0E−04	(m)
δ_e	1.0E−02	(m)
δ_s	1.0E−02	(m)
λ_m	0.2	(kW/m K)
λ_{air}	2.85E−02	(kW/m K)
ρ_m	836	(kg/m^3)

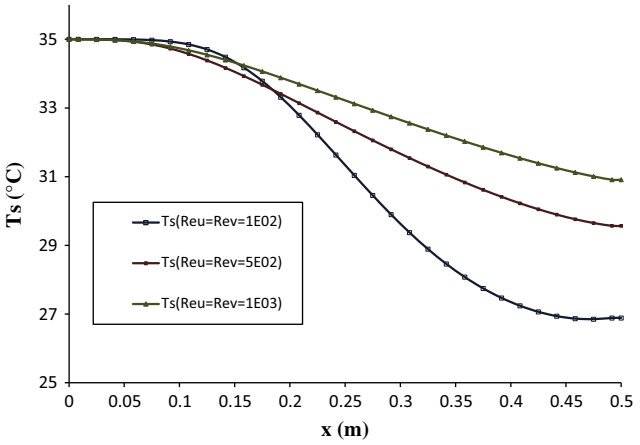

Fig. 7. Temperature profile at $y = 0.25$ m and $z = 5.10^{-3}$ m along the direction of the supply air stream (x-coordinate).

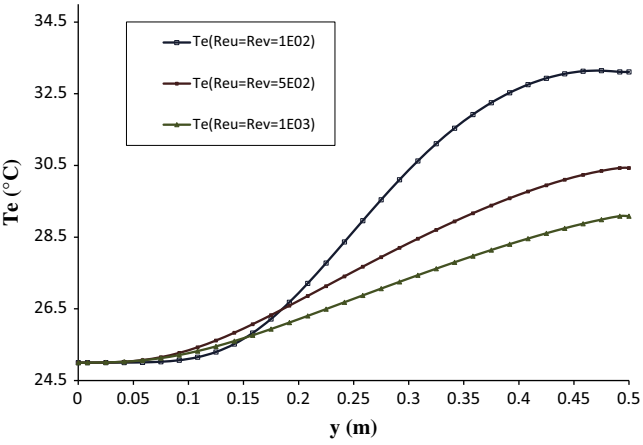

Fig. 8. Temperature profile at $x = 0.25$ m and $z = 5 \cdot 10^{-3}$ m along the direction of the (y-coordinate) exhaust air stream.

The temperature profiles along the x axis at $y = 0.25$ m and $z = 10^{-4}$ m are plotted in Fig. 13. The temperature difference between the two surfaces of membrane is in order of 10^{-4} °C because of the very small thickness.

Due to the small thickness of membrane, the temperature difference of membrane in thickness is very small compared to those in x and y directions. Therefore, conduction heat transfer in the membrane can be assumed to one dimensional in thickness direction. The variations of temperature difference between the two sides of membrane are nearly caused by the variation of temperature difference between the two air streams.

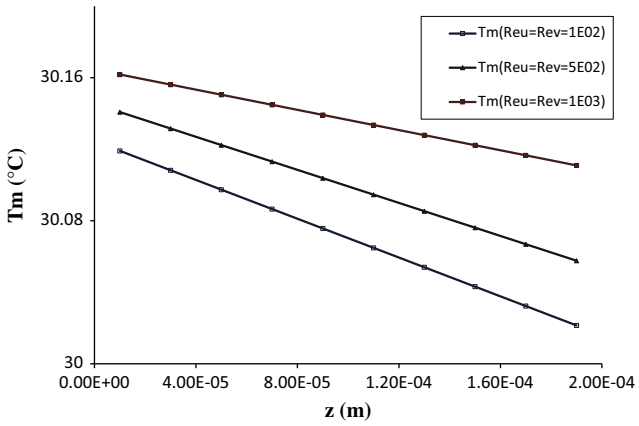

Fig. 9. Variation of the membrane temperature along the transversal coordinate (z) at $x = y = 0.25$ m.

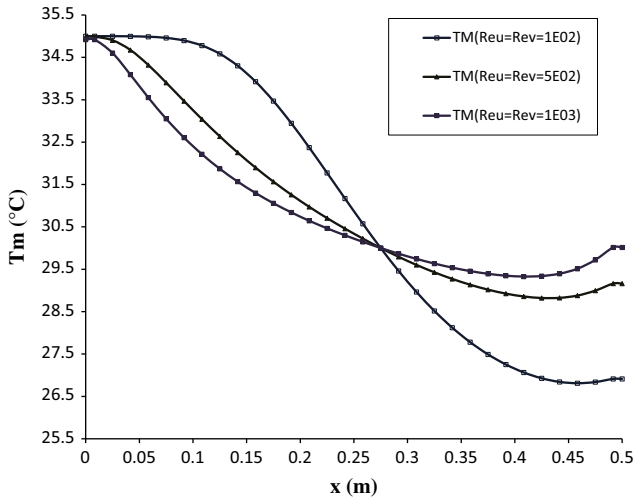

Fig. 10. Temperature profiles in membrane at $y = 0.25$ m and $z = 10^{-4}$ m along the direction of the supply air stream.

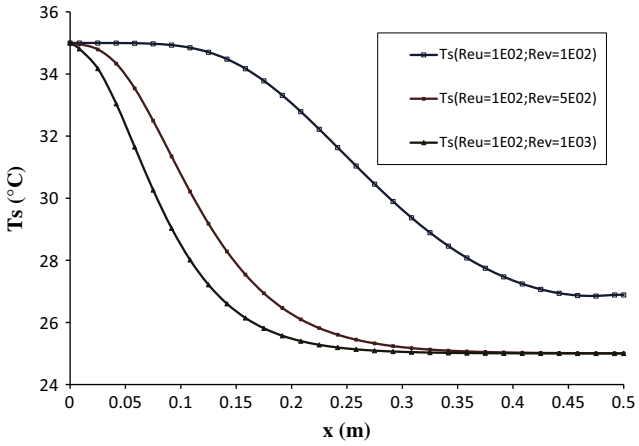

Fig. 11. Temperature profile at $y = 0.25$ m and $z = 5.10^{-3}$ m along the direction of the supply air stream (x-direction).

The temperature distribution in membrane in (x–y) plane at $z = 10^{-4}$ m for different Reynolds number are illustrated respectively in Figs. 14–16. For Reu = Rev = 10^2, the temperature contours in membrane are nearly parallel to the diagonal line and indicate

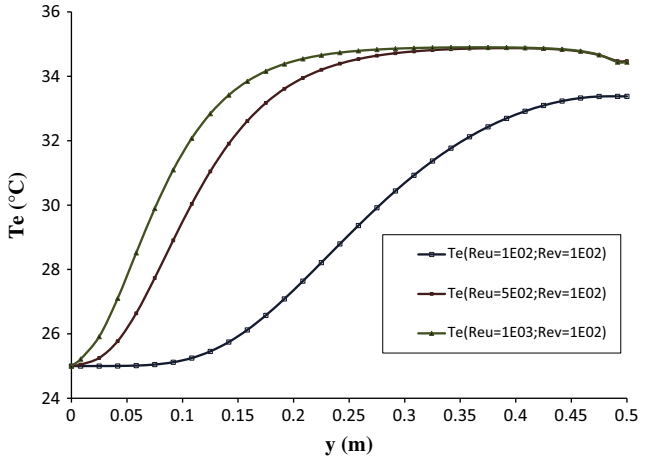

Fig. 12. Temperature profile at $x = 0.25$ m and $z = 5.10^{-3}$ m along the direction of the exhaust air stream (y-direction).

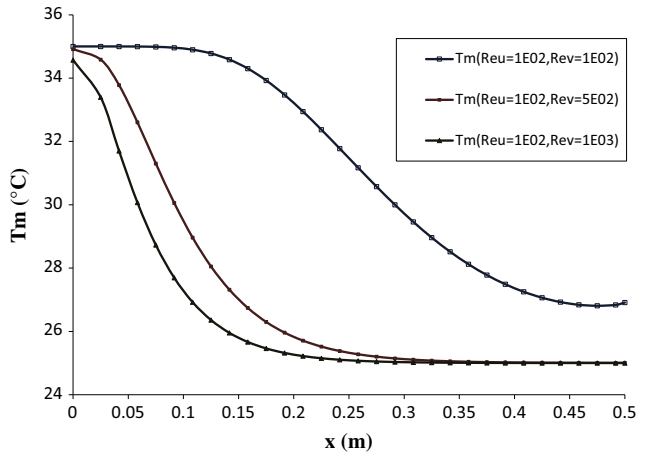

Fig. 13. Dimensionless temperature in membrane along the x-direction at $y = 0.25$ m and $z = 10^{-4}$ m.

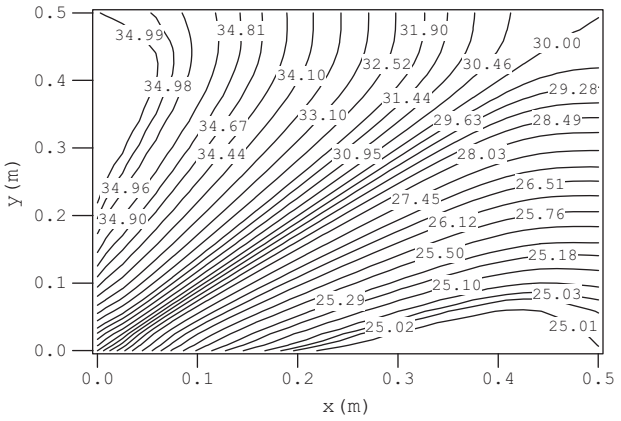

Fig. 14. Temperature distribution in membrane in (x–y) plane at $z = 5.10^{-3}$ m for Reu = Rev = 10^2.

that the temperature fields in two air streams are asymmetric. By further augmenting the Reynolds number value, the temperatures fields are nearly perpendicular to the x direction. The temperatures fields are maximum in (x–y) plane at $x = 0$ m and minimum in the outlet in (x–y) plane at $x = 0.5$ m.

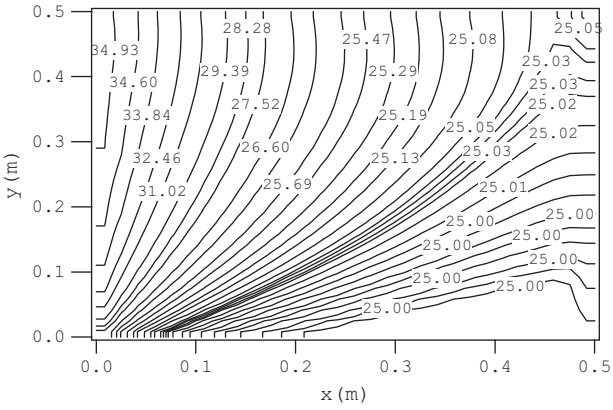

Fig. 15. Temperature distribution in membrane in (x–y) plane at $z = 5 \cdot 10^{-3}$ m for Reu = 10^2 and Rev = $5 \cdot 10^2$.

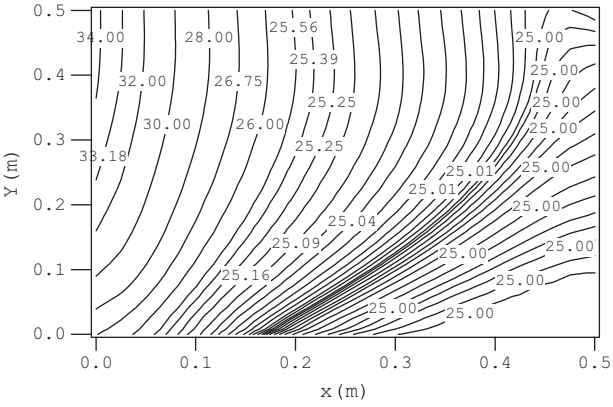

Fig. 16. Temperature distribution in membrane in (x–y) plane at $z = 5 \cdot 10^{-3}$ m for Reu = 10^2 and Rev = 10^3.

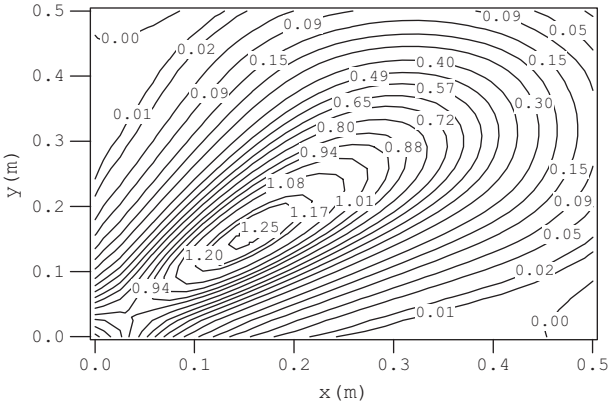

Fig. 17. Heat flux through the membrane at $z = 10^{-4}$ m for balanced flow (Reu = Rev = 10^2).

On another hand, for balanced flow (Reu = Rev), the contour values decrease along the diagonal line and the maximum flux is situated only on a small portion of membrane area near the inlets of the two air streams. For this reason, the membrane area is not effectively used in sensible heat exchangers. However, for unbalanced flow (Reu ≠ Rev) this problem is seen to be less significant. In addition, the boundary condition is neither uniform temperature

nor uniform heat flux surfaces (Figs. 17 and 18). Both, the temperature and the heat flux have a non uniform two-dimensional behavior.

3.3. Effectiveness

In a previous work [25], we presented the effect of total heat transfer on the sensible, latent and total effectiveness of balanced flow. These results indicate that the latent and total effectiveness decrease when the velocity increases and the sensible effectiveness remain constant. This indicates that moisture transfer through a membrane is more complicated and strongly dependent on operating parameters. Nasif et al. [26] have determined using temperature and moisture content measurements, the sensible, latent and total effectiveness of the heat exchanger. They employed the effectiveness as thermal performance indicators and incorporated in the modified software. The similarities between the equations for heat and mass transfer suggest that the empirical correlation for the mass transfer and humidity field would be similar to those for the heat transfer and temperature field. The concentration fields are not presented here because the same change is observed.

The wet airstream contains higher amount of moisture which builds up a higher partial vapor pressure; whereas the dry airstream contains lower amount of moisture and therefore has a lower partial vapor pressure. This pressure difference induced by the temperature difference between the two channels forms a driving force to the moisture transfer.

The sensible, latent and total effectiveness are defined by using the temperature variation method as follows [27]:

$$\varepsilon_s = \frac{(\dot{m}C_{pa})_s(T_{si}-T_{so})}{(\dot{m}C_{pa})_{\min}(T_{si}-T_{ei})}\ ; \quad \varepsilon_L = \frac{\dot{m}_s(w_{si}-w_{so})}{\dot{m}_{\min}(w_{si}-w_{ei})}\ ;$$
$$\varepsilon_{tot} = \frac{\dot{m}_s(H_{si}-H_{so})}{\dot{m}_{\min}(H_{si}-H_{ei})} \qquad (27)$$

For the unbalanced flow, we present the effectiveness for a Reynolds number relating to the supply canal fixed at Reu = 10^2 (Fig. 19) as a function of the Reynolds number Rev relating to the exhaust canal.

The effectiveness of the exchanger reaches its limiting and ideal value when Rev is increased. An increasing effectiveness is observed with an increasing Reynolds numbers Rev. The sensible, latent and total effectiveness's increases exponentially, for relatively low Rayleigh numbers (Reu = 10^2). However, the differences between effectiveness factors become smaller with an increasing Reynolds numbers. The differences in the effectiveness are seen to be higher at relatively large Reynolds number Rev.

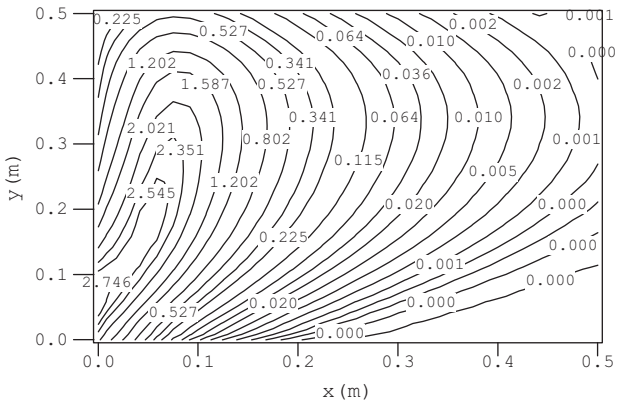

Fig. 18. Heat flux through the membrane at $z = 10^{-4}$ cm for unbalanced flow (Reu = 10^2 and Rev = 10^3).

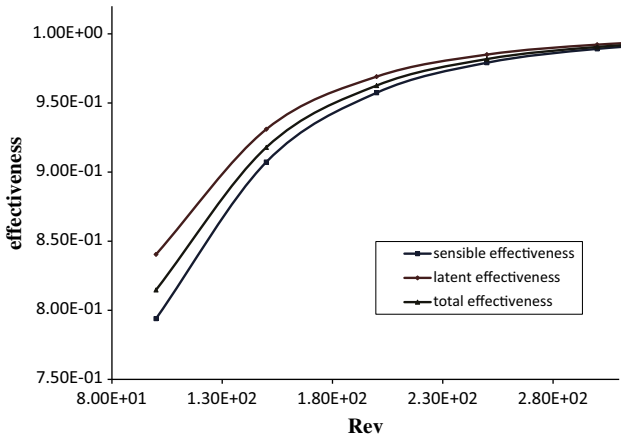

Fig. 19. Sensible, Latent and Total heat transfer effectiveness for Reu = 10^2.

These results also show that the moisture transfers process consumes some of the thermal energy which is not available for sensible transport. It is to be noted here that the line connecting the inlet conditions with outlet conditions in the psychometric chart is not horizontal due to the moisture transfer through the membrane. Furthermore, the total effectiveness is not a simple algebraic average of ε_S and ε_L but is a function of the ratio of latent to sensible energy differences.

4. Conclusion

A numerical model was developed to simulate the heat and mass transfer for the membrane based energy recovery ventilator. The influence of some operating parameters was analyzed. The temperature and humidity ratio profiles of air gas and membrane show that a transfer of heat and moisture is exhibited from one air stream to another. Furthermore, for cross flow arrangement, the directions for decreasing heat and mass fluxes are seen to be parallel to the diagonal line of the membrane. In addition, it is observed that the heat exchange is ideal for low Reynolds numbers. Hence, in order to gain high recovery efficiency it is necessary to decrease the Reynolds number for balanced flow and increase the Reynolds number for unbalanced flow. Besides, the unbalanced flow can overcome the problem of using small membrane area near the inlets. It is also concluded the unbalanced flow method is a good way to optimize the heat exchanger, by varying the air flow allowing energy saving and better heat and mass transfer.

References

[1] ASHRAE, Handbook: Fundamentals, American society of Heating, Refrigerating, and Air-Conditionning Engineers Inc., Atlanta, 1997.
[2] Nair Sankar, Verma Samir, Dhingra SC. Rotary heat exchanger performance with axial heat dispersion. Int J Heat Mass Transf 1998;41:2857–64.
[3] Frauhammer Jörg, Klein Harald, Eigenberger Gerhart, Nowak Ulrich. Solving moving boundary problems with an adaptive moving grid method: rotary heat exchangers with condensation and evaporation. Chem Eng Sci 1998;53:3393–411.
[4] Wang RZ, Wu JY, Xu YX, Teng Y, Shi W. Experiment on a continuous heat regenerative adsorption refrigerator using spiral plate heat exchanger as adsorbers. Appl Therm Eng 1998;18:P13–23.
[5] Hachemi A. Experimental study of thermal performance of offset rectangular plate fine absorber-plates. Renew Energy 1999;17:371–84.
[6] Manz H, Huber H. Experimental and numerical study of a duct/heat exchanger unit for building ventilation. Energy Build 2000;32:189–96.
[7] Zhang LZ. Convective mass transport in cross-corrugated membrane exchangers. J Membr Sci 2005;260:75–83.
[8] Zhang LZ. Heat and mass transfer in a cross-flow membrane-based enthalpy exchanger under naturally formed boundary conditions. Int J Heat Mass Transf 2007;50:151–62.
[9] Kadylak D, Cave Peter, Mérida Walter. Effectiveness correlations for heat and mass transfer in membrane humidifiers. Int J Heat Mass Transf 2009;52:1504–9.

[10] Zhang LZ. Heat and mass transfer in plate-fin sinusoidal passages with vapor-permeable wall materials. Int J Heat Mass Transf 2008;51:618–29.
[11] Fernández-Seara José, Diz Rubén, Uhía Francisco J, Dopazo Alberto, Ferro José M. Experimental analysis of an air-to-air heat recovery unit for balanced ventilation systems in residential buildings. Energy Convers Manage 2011;52:635–40.
[12] Zhang LZ, Liang Cai-Hang, Pei Li-Xia. Heat and moisture transfer in application scale parallel-plates enthalpy exchangers with novel membrane materials. J Membr Sci 2008;325:672–82.
[13] Zhang LZ. Coupled heat and mass transfer through asymmetric porous membranes with finger-like macrovoids structure. Int J Heat Mass Transf 2009;52:751–9.
[14] Mahmud K, Mahmood Gazi I, Simonson Carey J, Besant Robert W. Performance testing of a counter-cross-flow run-around membrane energy exchanger (RAMEE) system for HVAC applications. Energy Build 2010;42:1139–47.
[15] Zhang LZ. Conjugate heat and mass transfer in membrane-formed channels in all entry regions. Int J Heat Mass Transf 2010;53:815–24.
[16] Zhang Tao, Liu Xiao-Hua, Zhang Lun, Jiang Yi. Match properties of heat transfer and coupled heat and mass transfer processes in air-conditioning system. Energy Convers Manage 2012;59:103–13.
[17] Vaz J, Sattler Miguel A, dos Santos Elizaldo D, Isoldi Liércio A. Experimental and numerical analysis of an earth–air heat exchanger. Energy Build 2011;43:2476–82.
[18] Al-Waked Rafat, Nasif Mohammad Shakir, Morrison Graham, Behnia Masud. CFD simulation of air to air enthalpy heat exchanger. Energy Convers Manage 2013;74:377–85.
[19] Wiliam H. Press, Saul A. Teukolsky, Wiliam T. Vetterling, Brian P. Flannery. Numerical Recipes in Fortran 90: The art of parallel Scientific Computing. 2nd ed., Cambridge University Press, 1986–2001.
[20] Suhas V. Patankar. Numerical Heat Transfer and Fluid Flow. In: 5th Ed. ed., Handbook of series in computational methodes in mechanics and thermal sciences. Minkowyez WJ, Sparrow EM, editors, New York, 1980, ISBN 0-07-048740-5.
[21] S.V. Patankar. Numerical Methods for Heat and Fluid Flow, 1980, p. 107.
[22] Chouikh R, Ben Snoussi L, Guizani A. A Numerical study of the heat and mass transfer in inclined glazing cavity: application to a solar distillation cell Renewable Energy, vol. 32. September, 2006, p. 1511–24.
[23] Alimi W, Chouikh R, Guizani A. A Modelling of concentration and current distribution in a PEMFC single cell Progress in Computational. Fluid Dyn 2008;8(6):362–71.
[24] Tiss F, Chouikh R, Guizani A. A numerical investigation of the effects of membrane swelling in polymer electrolyte fuel cells. Energy Convers Manage 2013;67:318–32.
[25] Sebai R, Chouikh R, Amara K, Guizani A. Numerical study of heat and mass transfer in a porous membrane used in energy recovery devices. International Review on Modelling and Simulations (I.RE.MO.S.), vol. 4(4). 2011. p. 1945–51.
[26] Nasifa M, AL-Wakedc R, Morrisona G, Behniad M. Membrane heat exchanger in HVAC energy recovery systems, systems energy analysis. Energy Build 2010;42:1833–40.
[27] Bayazitoglu Y, Ozigik MN. Elements of heat transfer. New York: MC-Craw Hill; 1988. p. 433.